

# Optimization and Parametric Study of the Cap Geometry on Collapse Properties of Energy Absorbers under Quasi-static Loading

S. Chahardoli<sup>a</sup>, N. Vahdat Azad<sup>b,\*</sup>

<sup>a</sup> Mechanical Engineering Department, Bu-Ali Sina University, Hamedan, Iran.

<sup>b</sup> Aeronautical Engineering Department, Shahid Sattari University, Tehran, Iran.

## Article info

### Article history:

Received 27 February 2019

Received in revised form

22 June 2019

Accepted 27 July 2019

### Keywords:

Energy absorber

LS-DYNA

Quasi-static loading

Optimization

## Abstract

In the present research, the influence of cap geometry on the collapse of thin-walled aluminum-made energy absorbers with various section geometries was investigated. For this purpose, a total of 35 different absorbers were subjected to axial quasi-static loading. In this respect, five different section types and seven different cap configurations were considered for the absorbers and their caps, respectively. The analyses were performed in both experimental and numerical methods. The numerical simulations were conducted using LS-DYNA Software and experimental tests were performed to verify the numerical investigations. Good agreement was obtained between the experimental data and numerical results. The results indicated that, in all cases, the application of the cap enhanced the crush force efficiency while lowering maximum force at collapse. In the final stage of the research, optimal absorbers for the cases with open-ended and close-ended caps were proposed using Minitab Software based on the response surface methodology.

## 1. Introduction

Thin-walled structures enjoy significant advantages in terms of light weight and energy absorption capacity so that they are widely applied in automotive, aerospace, transportation, and military industries. These structures absorb energy by plastic deformation. Various parameters have been defined to determine collapse characteristics of an energy absorber, including specific energy absorption (SEA, pertaining to the entire duration of the collapse phenomenon), maximum force ( $F_m$ , usually occurring at the start of the collapse phenomenon), and crush force efficiency (CFE, a measure of impact stability in a hitting phenomenon; evaluated by dividing average force ( $F_a$ ) over the force-displacement curve by the maximum force).

During the past years, numerous pieces of research have been performed on collapse characteristics of such absorbers via numerical, analytical and experimental methodologies [1-6]. One of the topics discussed in such research works is to decrease the maximum force at collapse and increase energy absorption capacity. In this respect, one may refer to the following references, most of which have considered such energy absorbers under quasi-static loading. Zhang et al. [7] investigated axial collapse of cylindrical tubes with a leverage as buckling initiator. This buckling initiator was used to decrease the initial force required for corrugating thin-walled circular tubes under axial loading. In another research, Acar et al. [8] investigated symmetrically corrugated truncated cones using a multi-objective optimization algorithm. Shariati and Allahbakhsh [9] focused on nu-

\*Corresponding author: N. Vahdat Azad (Assistant Professor)  
E-mail address: nader.vahdatazad@ssau.ac.ir  
<http://dx.doi.org/10.22084/jrstan.2019.18577.1089>  
ISSN: 2588-2597

merical and experimental investigation of buckling and post-buckling of steel-made hemispherical shells and evaluated average buckling force. Alavi Nia and Haddad Hamedani [10] performed a comparative analysis, both experimentally and numerically (simulation), on energy absorption and deformation of thin-walled columns by different section geometries (e.g. circular, square-shaped, rectangular, hexagonal, triangular, pyramid-shaped, and conical). Ghamarian and Farsi [11] examined, both experimentally and numerically, axial collapse of thin-walled composite structures, and further considered the influences of introducing a cap on collapse behavior of cylindrical and conical thin-walled structures.

In another work, Ghamarian and Tahaye Abadi [12] examined both experimentally and numerically, the collapse of close-ended cylindrical shells filled with foam under axial loading. They showed that capped cylindrical shells are better energy absorbers as compared to uncapped cylindrical shells. Jandaghi Shahi and Marzbanrad [13] studied the collapse behavior of thin-walled aluminum structures with circular section and variable wall thickness under quasi-static axial loading. They demonstrated that one can improve energy absorption capacity and maximum force at collapse by changing the wall thickness. Song [14] studied thin-walled structures with windows on its wall and checked the effects of the windows dimensions on the collapse characteristics. Sun et al. [15] demonstrated that, compared to conventional columns, the columns with functionally graded thickness (FGT) exhibit higher specific energy absorption and lower maximum force under impact loading. Based on an experimental study, Sharifi et al. [16] demonstrated that, in two-tube absorbers, the maximum force at collapse can be reduced by thinning the shell edges. Alavi Nia and Chahardoli [17] optimized the height difference in nested three-tube structures in an attempt to decrease maximum force while enhancing the specific energy absorption.

Researchers have consistently sought lower maximum force at collapse and higher CFE. However, despite the numerous efforts made to achieve such a target, a comprehensive solution is yet to be presented. The present study adopts caps of different geometries to reduce maximum force at collapse while improving CFE. In this paper, the effect of each geometry on col-

lapse characteristics was studied and optimal caps were identified using response surface methodology (RSM) optimization.

## 2. Materials and Tests

In this section, the considered materials were tested to identify their characteristics. The absorbers considered in this research were made of aluminum plates of 1.5mm thickness. The plates were subjected to quantummetry test. Table 1 reports the chemical composition of the aluminum alloy. According to Ref. [18], the plate was made from aluminum 1100. According to ASTM-E8 standard [19], for the sake of tensile testing, two specimens were cut from the plate using a wire-cut machine and were then subjected to tensile loading on a 15-ton SANTAM apparatus. Fig. 1a shows the cut specimen of the aluminum plate for tensile testing. The type of fracture occurred to the specimen (at 45°) indicated that the used plate was made of a ductile material. Fig. 1b shows the actual stress-strain curve extracted from the force-displacement diagram obtained using SANTAM apparatus. Table 2 presents the mechanical characteristics extracted from the stress-strain curve.

## 3. Simulation

LS-DYNA is powerful simulation software for energy absorbers and has been widely used in many studies. In this section, a number of specimens were simulated utilizing LS-DYNA software. Fig. 2 demonstrates the simulated model of one of the absorbers considered in this research, as an example. All of the simulated absorbers are 120mm in height. According to Fig. 2, each absorber was simulated as a shell placed between two rigid jaws. Dimensions of the shell elements are 2×2mm. The size of shell elements was set after mesh convergence. The lower jaw was assumed to be fixed, while the upper jaw compressed the absorber quasi-statically until displacement of 100mm.

No speed is defined in quasi-static simulations. In fact, in LS-DYNA code, it is possible to do a quasi-static analysis by running a regular explicit simulation, invoking mass-scaling option as necessary to crank out the results in a reasonable timeframe, but this approach can pose some challenges.

**Table 1**  
Chemical composition of the aluminum alloy comprising the rolled plate.

Element	Si + Fe	Cu	Mn	Zn	Others (each)	Others (total)	Al
Percent for 1100 [18]	1.0 (Max)	0.05 To 0.2	0.05 (Max)	0.1 (Max)	0.05 (Max)	0.15 (Max)	Rem
Percent for Plate	0.1 + 0.29	trace	0.005	0.01	✓	✓	✓

**Table 2**  
The mechanical characteristics extracted from the true stress-strain curve demonstrated in Fig. 1.

Young modulus (E) (GPa)	Yield stress ( $\sigma_y$ ) (MPa)	Ultimate stress ( $\sigma_U$ ) (MPa)	Fracture strain
70	0.047	187.5	175.3

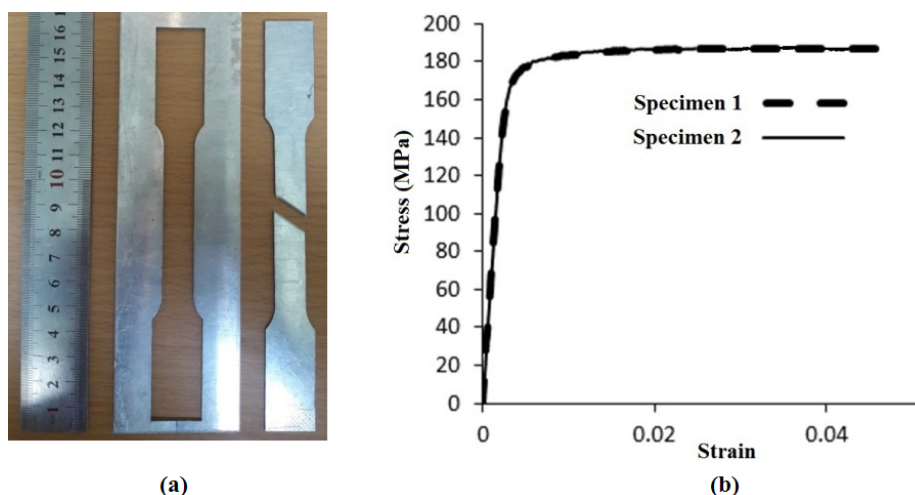


**Fig. 1.** Tensile testing: a) Tensile testing specimen, b) True stress-strain curve of the aluminum 1100, (Speed 2mm/min).

**Table 3**  
Geometric characteristics of the simulated main tubes.

					
Height (mm)	90	90	90	90	90
Polygonal side/circle radius (mm)	62.8	47.1	37.7	31.4	30
Cross-sectional perimeter (mm)	188.4	188.4	188.4	188.4	188.4
Cross-sectional surface (mm <sup>2</sup> )	1708	2218	2445	2562	2827

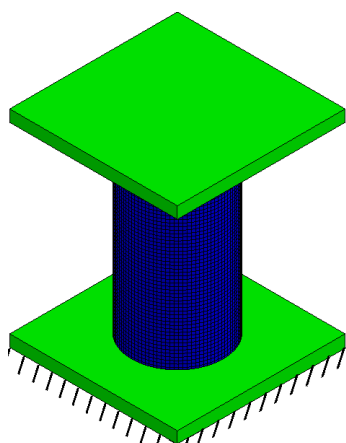


**Fig. 2.** An example of simulated energy absorber.

One has to keep an eye on the kinetic energy in the system to minimize the inertial effects. Basically, the kinetic energy should remain small relative to the internal energy. Mass-scaling refers to the load applied faster than that of the quasi-static experiment in order to reduce the simulation time.

Solid material model was adopted for the lower and upper jaws, while the shells were simulated using Mat-Piecewise-Linear-Plasticity ma-

terial model. The contact between the jaws and shell and also the contact between the absorber elements were simulated using two friction models, namely CONTACT-AUTOMATIC-SURFACE-TO-SURFACE and CONTACT-AUTOMATIC-SINGLE-SURFACE models, respectively. In these models, static and dynamic friction coefficients were set to 0.3 and 0.2, respectively.

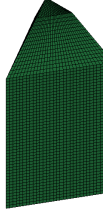
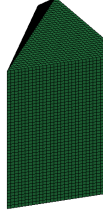
### 3.1. Simulated Specimens

Simulated specimens are presented in this section. A total of 35 various specimens were simulated. Each specimen was composed of two parts, main tube and a cap. Five different geometries (triangular, square-shaped, regular pentagonal, regular hexagonal, and circular) were considered for the main tube, while seven different types of cap were studied for each main tube. Height and perimeter of all main tubes were identical: 90 and 188.4mm, respectively. Table 3 shows the simulated main tubes along with their geometric characteristics.

All the studied caps were 30mm in height, with their lower base being of the same geometry as that

of the section of the simulated main tube in Table 3. The three former caps were open-ended, while the latter four caps had their ends closed. The measure of the upper base of the caps (radius of the circle) is reported in Table 4. This table presents all of the 35 simulated specimens along with geometrical characteristics of the upper base of the caps.

**Table 4**  
Geometric characteristics of the used caps.

							
Name	TOE1	TOE2	TOE3	TCE1	TCE2	TCE3	TCE4
Upper side	62.8	31.4	20.9	62.8	31.4	20.9	0
Cap height	30	30	30	30	30	30	30
							
Name	QOE1	QOE2	QOE3	QCE1	QCE2	QCE3	QCE4
Upper side	47.1	23.6	15.7	47.1	23.6	15.7	0
Cap height	30	30	30	30	30	30	30
							
Name	POE1	POE2	POE3	PCE1	PCE2	PCE3	PCE4
Upper side	37.7	18.8	12.6	37.7	18.8	12.6	0
Cap height	30	30	30	30	30	30	30
							
Name	HOE1	HOE2	HOE3	HCE1	HCE2	HCE3	HCE4
Upper side	31.4	15.7	10.5	31.4	15.7	10.5	0
Cap height	30	30	30	30	30	30	30
							
Name	COE1	COE2	COE3	CCE1	CCE2	CCE3	CCE4
Upper radius	30	15	10	30	15	10	0
Cap height	30	30	30	30	30	30	30

**Table 5**  
Collapse characteristics of the simulated specimens.

	Specimen	Crushing length (mm)	SEA (J/g)	Fm (kN)	Fa (kN)	CFE (%)
Open end	TOE1	100	14.2	47.4	12.9	27.2
	TOE2	100	15.5	19.1	13.4	70.2
	TOE3	100	15.4	19.7	13.1	66.5
	QOE1	100	14	49.5	12.7	25.7
	QOE2	100	17	25	14.7	58.8
	QOE3	100	16.5	30.2	14.1	47
	POE1	100	19.4	50.9	17.9	35.2
	POE2	100	18.1	30.4	15.8	52
	POE3	100	17.7	26.6	15.4	57.9
	HOE1	100	20.1	50.2	18.1	36.1
	HOE2	100	18.5	33.7	15.9	47.2
	HOE3	100	17.6	31.1	15	48.2
	COE1	100	22.4	49.5	20.4	41.2
	COE2	100	20.8	38.3	18.2	47.5
	COE3	100	19	43.9	16.5	37.6
Capped end	TCE1	100	14.2	44.8	13.9	31
	TCE2	100	15.3	22.7	13.5	59.5
	TCE3	100	15.6	25.2	13.3	52.8
	TCE4	100	13.7	24	11.2	46.7
	QCE1	100	16.1	48.3	16	33.1
	QCE2	100	17.2	30.1	15.3	50.8
	QCE3	100	16.3	30.2	14.1	46.7
	QCE4	100	16	33.2	13.2	39.8
	PCE1	100	17.5	50.6	17.9	35.4
	PCE2	100	17.7	35.6	15.9	44.7
	PCE3	100	17.4	33.4	15.3	45.8
	PCE4	100	16.6	37.4	14	37.4
	HCE1	100	18.6	50.2	18.6	37.1
	HCE2	100	18.2	39.2	16.2	41.3
	HCE3	100	17.7	35.3	15.2	43.1
	HCE4	100	17.1	38.6	14.1	36.5
	CCE1	100	20.8	49.4	21.3	43.1
	CCE2	100	18.8	42.6	17	39.9
CCE3	100	19.9	44.5	17.5	39.3	
CCE4	100	18.2	48.3	15.4	31.9	

According to Table 4, it is obvious that all the specimens in each column of the table were identical in the perimeters of the main tube and upper base of the cap. Given that all of the specimens were of the same height, one may conclude that the specimens with the same type of cap have approximately identical masses irrespective of the geometry of their sections. The simulated specimens listed in Table 4 were subjected to quasi-static axial loading, and their collapse characteristics were extracted based on their force-displacement curves. Table 5 shows collapse characteristics of all the 35 simulated specimens. According to Tables 4 and 5, a combination of letters and numbers was used for naming the specimens considered in this research. Accordingly, the first letter indicates general geometry of the section (triangular, square-shaped, regular pentagonal, regular hexagonal, and circular), while the second and third letters indicate whether the cap is open-ended or close-ended. Moreover, three and four cases were considered with open-ended and close-ended caps, respectively, with each case being denoted by a number.

### 3.2. Validation

Among the specimens listed in Table 5, the specimens TOE1, QOE1, POE1, and HOE1 were prepared experimentally. In order to construct these specimens, rectangular specimens of the plate were cut by a guillotine and were then formed into the final absorber by argon welding. Fig. 3 shows the image of experimental specimens. The test specimens were subjected to quasi-static loading using SANTAM apparatus. The loading speed in tests was 2mm/min.

Plotted in Fig. 4 are force-displacement curves for the specimens TOE1, QOE1, POE1, and HOE1 based on experimental data and numerical results. In Table 6, collapse characteristics of the absorbers were compared and their differences were expressed in percentages. Experimental and numerical demonstrations of the collapsed absorbers are shown in Fig. 5. The side view of the tested and simulated specimens is shown in Figs. 6, 7 presents the stages through which the HOE1 was collapsed experimentally.



**Fig. 3.** Prepared test specimens for verifying the simulation results.

As shown in Figs. 4, 5 and 6 and also Table 6,

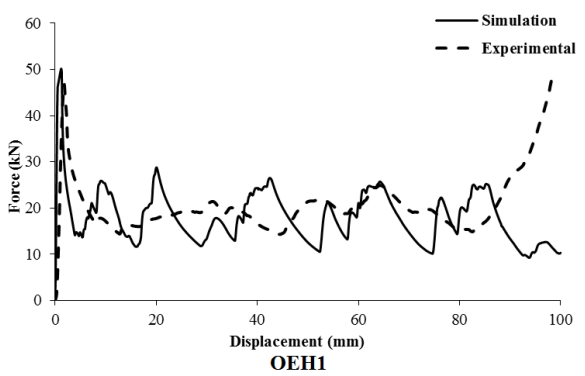
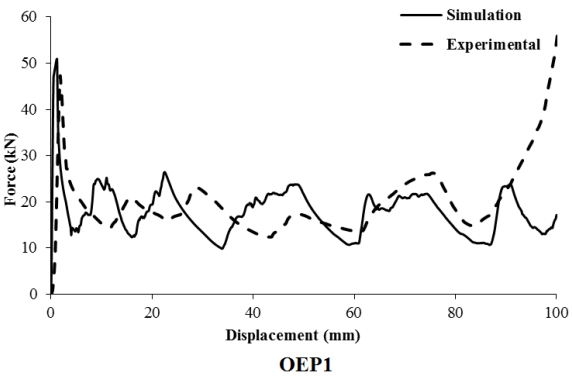
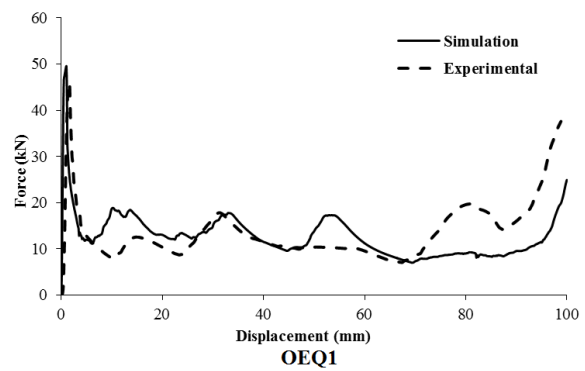
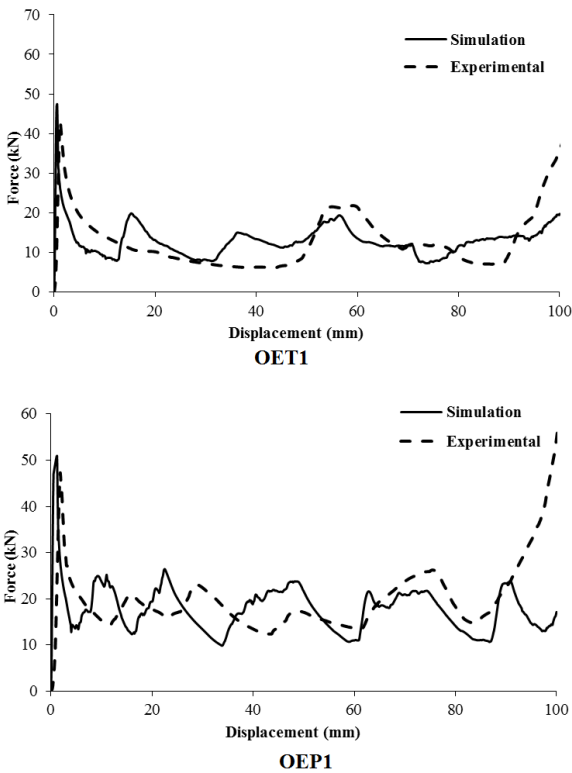


**Fig. 4.** Force-displacement curves of the specimens TOE1, QOE1, POE1, and HOE1, as per experimental and numerical studies.

a good agreement was obtained between the experimental data and numerical results. However, there are some differences between experimental and numerical results such as folds numbers which can be due to some reasons as follow: (a) Argon welding method leads to the creation of anisotropy in the structure's body, (b) Argon welding method creates unexpected curvature in the structure's body, (c) Shell model is used for simulation of absorbers, but in fact, they are not an exact shell, (d) In simulated specimens, thickness is permanent all over the structures, but in real states, they do not have the same thickness in their body. It must be mentioned that welding lines can't be considered in simulations because of three main reasons: (a) Simulation of welding line can only be done using extraction of material properties in the welding zone. (b) In a welded sample, the thickness of the weld line varies from one point to another point, and therefore, in any simulation, there are inevitable differences. (c) The area of the welding line in the experimental samples is low compared to the area without welding, and thus welding line in numerical simulations can be ignored.

#### 4. Results and Discussion

In this section, the results obtained from the numerical simulations were compared. To this end, the data reported in Table 5 were graphically demonstrated in the form of plots to check the effect of each character on the collapse characteristics.

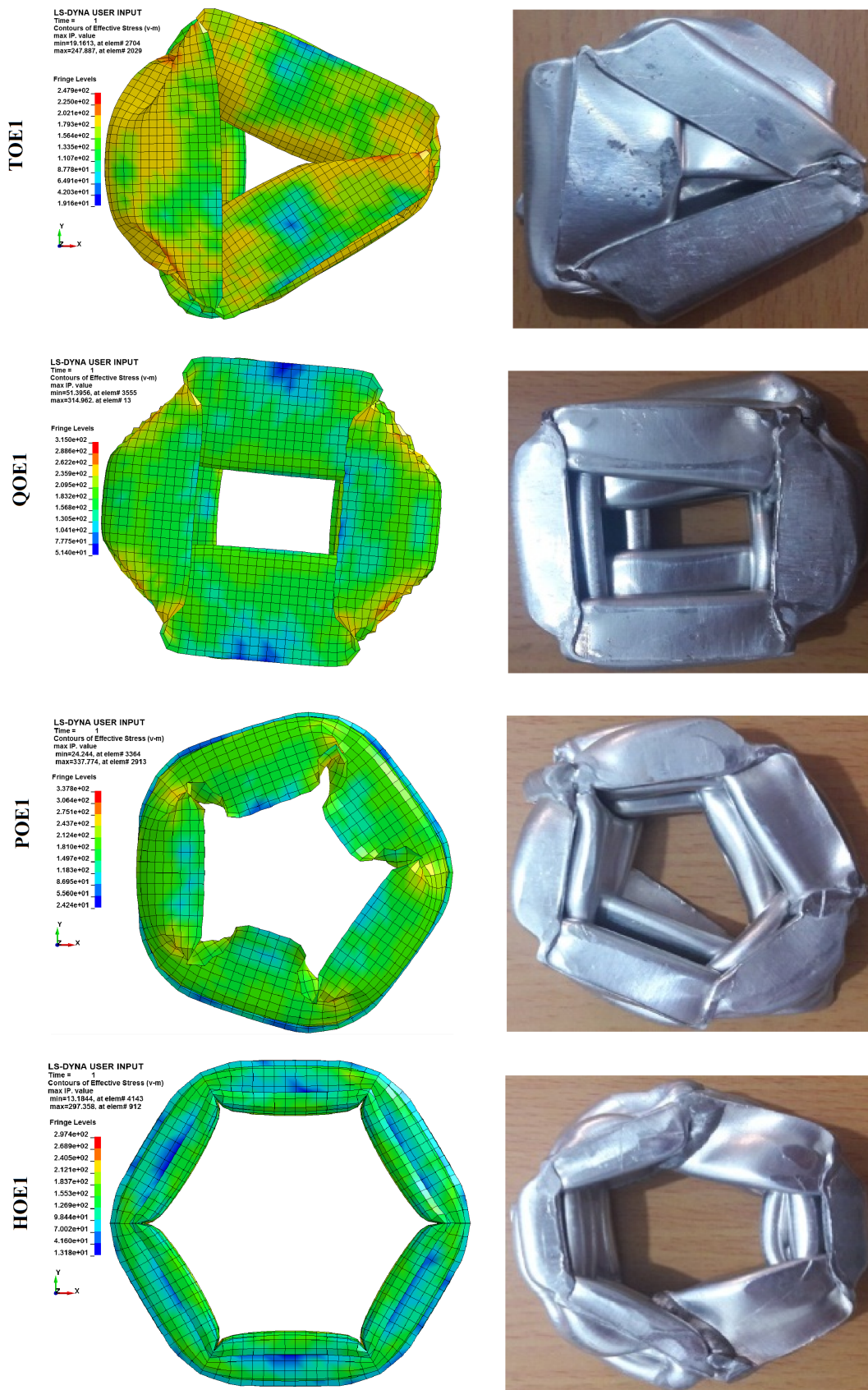
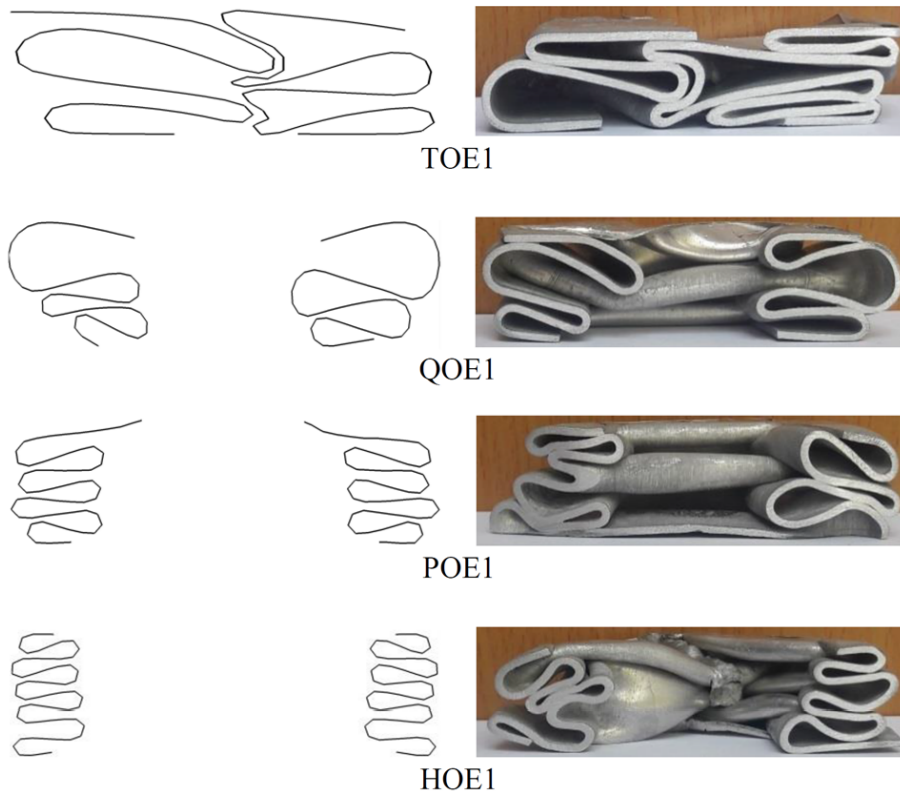
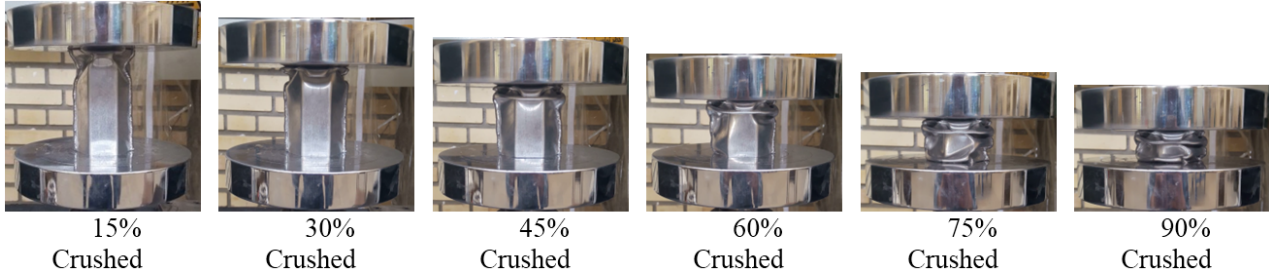


Fig. 5. Demonstrations of collapsed absorbers, as per experimental and numerical studies.



**Fig. 6.** Side view of the tested and simulated specimens.



**Fig. 7.** Different stages of HOE1 collapse in experimental state.

**Table 6**

Verification of the simulation results by comparing those to the corresponding experimental data.

Specimen code	Energy (J)			Fm (kN)			Fa (kN)		
	Experimental	Simulation	Difference (%)	Experimental	Simulation	Difference (%)	Experimental	Simulation	Difference (%)
OET1	1383.1	1294.9	-6.4	44.1	47.4	7.5	13.8	12.9	-6.5
OEQ1	1367	1272.1	-7	45.9	49.5	7.8	13.7	12.7	-7.2
OEP1	1931.1	1785.8	-7.5	47.8	50.9	6.5	19.3	17.9	-7.2
OEH1	1949.9	1806.6	-7.3	48	50.2	4.6	19.5	18.1	-7.2

#### 4.1. Effect of Cap Geometry

As mentioned before, two types of cap (open-ended and close-ended) were considered in the main tubes of various sectional geometries. Fig. 8 shows the effects

of different types of the cap on the collapse characteristics. According to Fig. 8a, in all the three cases, a change in the main tube section from triangular to circular led to enhanced specific energy absorption for

the absorbers with open-ended caps,. This was also the case with the absorbers with close-ended caps, i.e. a larger amount of energy could be absorbed by chang-

ing the form of the main tube section from triangular to circular.

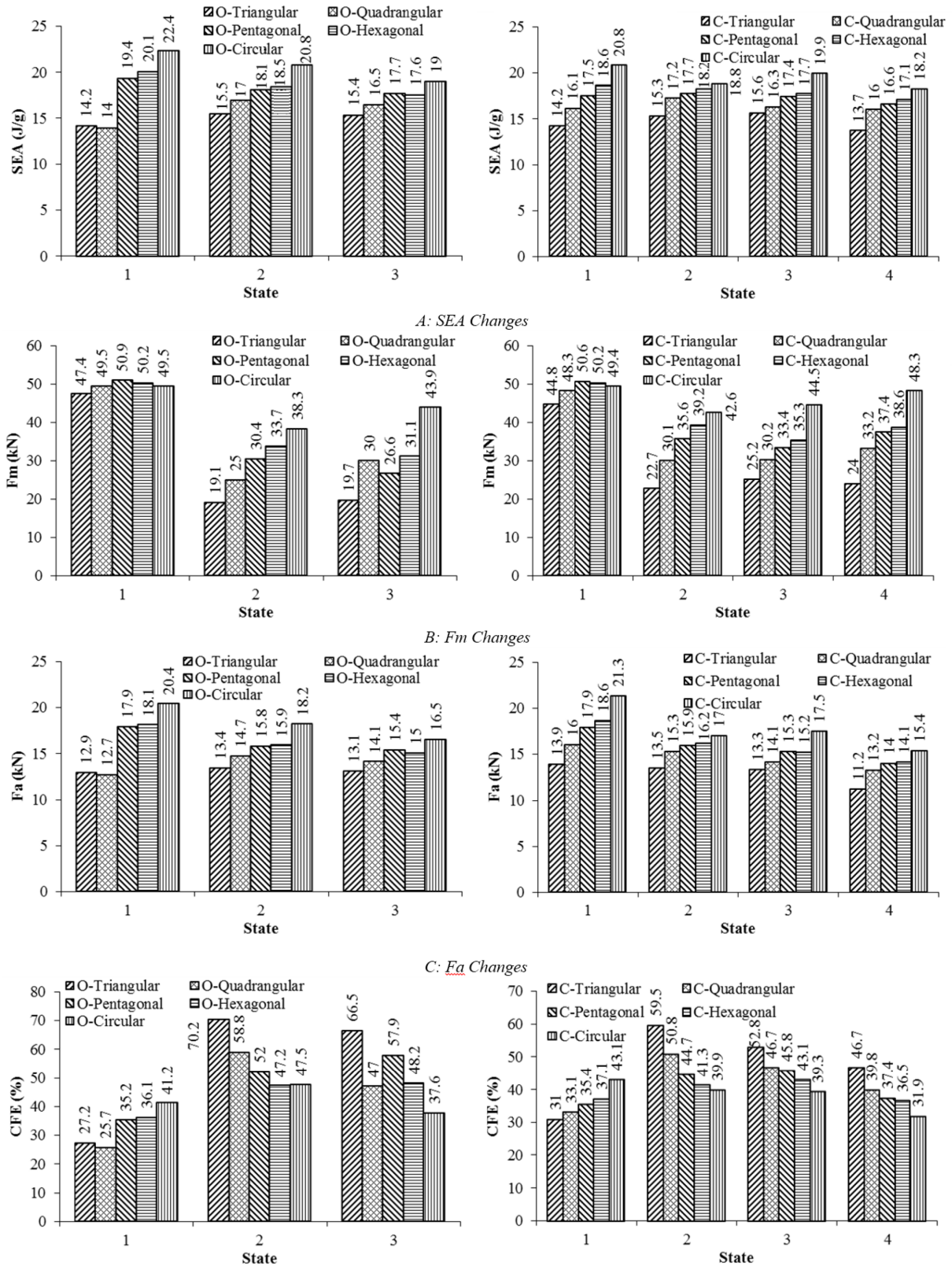
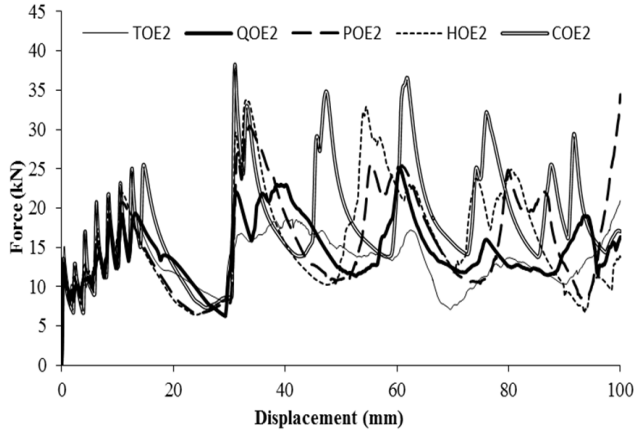


Fig. 8. Effect of different cap configurations (open-ended or close-ended) on collapse characteristics.

As shown in Fig. 8b, a change from triangular section to circular section added to the maximum force at collapse for all the open-ended and close-ended sections. This also held true for average force values. Force-displacement curves of the specimens TOE2, QOE2, POE2, HOE2, and COE2 are shown in Fig. 9.



**Fig. 9.** Force-displacement curves for TOE2, QOE2, POE2, HOE2, and COE2 absorbers.

Based on Fig. 8d, for all cases with either open-ended or close-ended caps (except for Case 1), lower CFE was observed as the main tube section changed from triangular to circular. Case 1, however, exhibited enhanced CEF upon such a change. According to Figure 7d, the highest CFE (70.2%) is for TOE2 specimen. Fig. 10 presents force-displacement curves of the specimens CCE1, CCE2, CCE3, and CCE4. Based on Fig. 8, the use of cap clearly enhanced CFE and decreased maximum force at collapse in all cases.

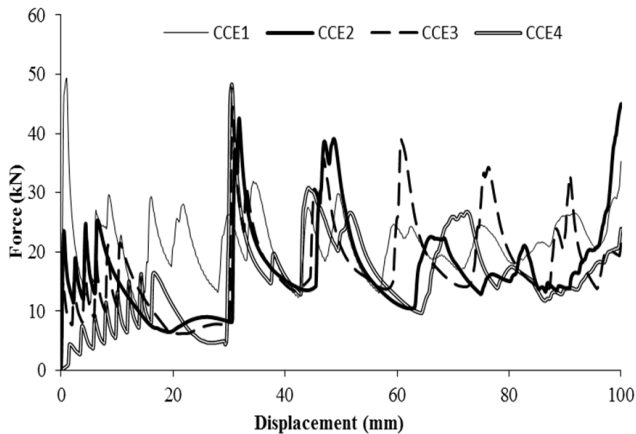


**Fig. 10.** Force-displacement curves for CCE1, CCE2, CCE3, and CCE4 absorbers.

According to Fig. 8, SEA and CFE values for open-end specimens are greater than those of close-ended ones. Force-displacement curve of CCE2 and CCO2 are shown in Fig. 11 for SEA. According to this figure, the underlined area in open-ended specimen is greater than that of the close-ended one, and thus it is expected

that more SEA is recorded for open-ended type which is because of folding mode in crushing. Previous studies have showed that diamond mode in folding has more energy absorption than axisymmetric mode. Close-ended structures would fold in axisymmetric mode by having more constraint in top of their body, but open-ended structures fold in diamond mode.

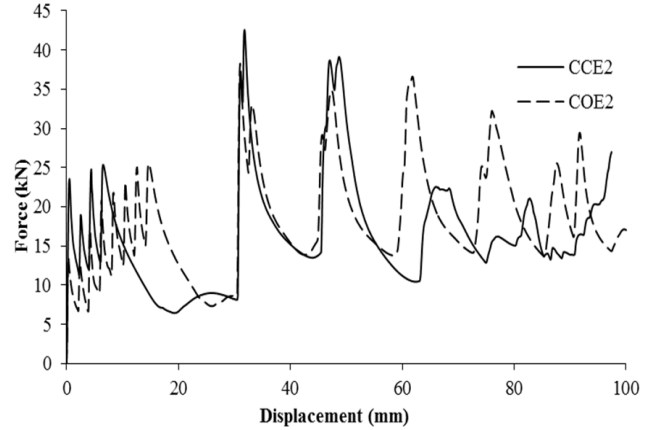


**Fig. 11.** Force-displacement curves for CCE2, COE2 absorbers.

Also, it must be mentioned that close-ended absorbers have more mass than open-ended types, and therefore, in the same energy absorption, more SEA is expected for open-ended type.

Constraints in close-ended structures would raise the maximum force, and thus, for specimens which have small amount of energy absorption (or in other words small amount of average force in similar length of crushing), more  $F_m$  and less  $F_a$  leads to less CFE in close-end structures relative to open-ended structures.

#### 4.2. Optimization

In this section, the data presented in Table 5 was used for optimization. Minitab software was used for this purpose. General algorithm of the multi-objective optimization based on RSM is shown in Fig. 12. Two parameters were considered as the main factors characterizing the absorber geometry: (1) the ratio of area-to-perimeter for main tube of the absorber, which is defined by Eq. (1), and (2) the ratio of area-to-perimeter for small base of cap, which is defined by Eq. (2).

$$a = \frac{\text{Area of man tube of the absorber}}{\text{Perimeter of main tube of the absorber}} \quad (1)$$

$$b = \frac{\text{Area of small base of cap}}{\text{Perimeter of small base of cap}} \quad (2)$$

##### 4.2.1. Optimization of Absorbers with Open-ended Caps

Table 7 lists the parameters used to optimize the absorbers with open-ended cap. Using response surface

methodology (RSM), two quadratic equations were determined for specific energy absorption and maximum force at collapse of the absorbers with open-ended caps. These two equations are expressed as Eqs. (3) and (4), respectively. Indicated beside each equation is the corresponding value of R2, which refers to the sum of squares error. Fig. 13 demonstrates the surfaces fitted for the specific energy absorption and maximum force at collapse along with the respective contours.

Fig. 14 shows the results of multi-objective optimization via RSM. The figure demonstrates the optimal configuration for the absorbers with open-ended caps. Based on this figure, the absorber with “a” and “b” values of 15 and 11.92 was expected to exhibit specific energy absorption and maximum force at collapse of 22.5 and 40, respectively. The value of the parameter “a” (15) refers to a circular form for the main tube section, while the value of the parameter “b” (11.92) defines a circular cap with an upper base of 23.84mm in radius. In order to verify the utilized optimization method, the proposed absorber via RSM was simulated in LS-DYNA. Table 8 compares the results of RSM with the outputs of LS-DYNA, indicating the capability of the RSM in predicting the optimal configuration for open-ended structures.

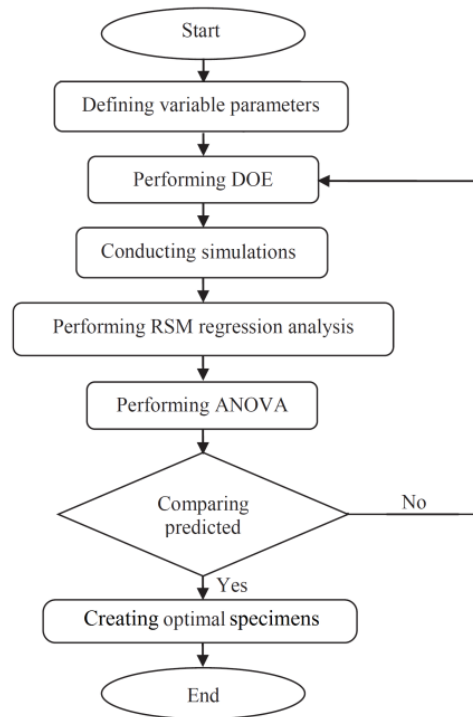


Fig. 12. General algorithm of the multi-objective optimization based on RSM.

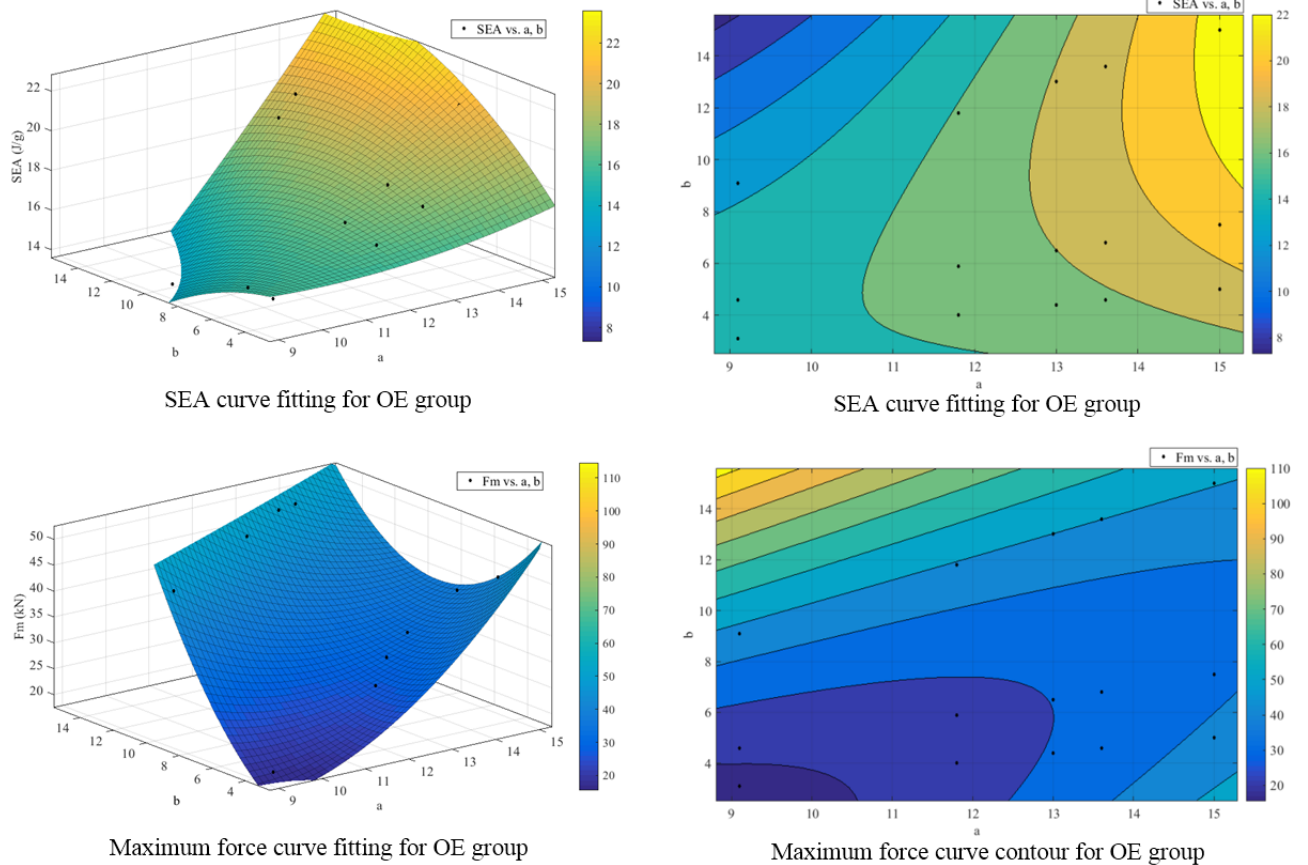


Fig. 13. The fitted curve and corresponding contours for specific energy absorption and maximum force at collapse of OE absorbers.

**Table 7**  
The parameters used to optimize the absorbers with open-ended cap.

Specimen	A	B	SEA (J/g)	Fm (kN)	CFE (%)
TOE1	9.1	9.1	14.2	47.4	27.2
TOE2	9.1	4.6	15.5	19.1	70.2
TOE3	9.1	3.1	15.4	19.7	66.5
QOE1	11.8	11.8	14	49.5	25.7
QOE2	11.8	5.9	17	25	58.8
QOE3	11.8	4	16.5	30.2	47
POE1	13	13	19.4	50.9	35.2
POE2	13	6.5	18.1	30.4	52
POE3	13	4.4	17.7	26.6	57.9
HOE1	13.6	13.6	20.1	50.2	36.1
HOE2	13.6	6.8	18.5	33.7	47.2
HOE3	13.6	4.6	17.6	31.1	48.2
COE1	15	15	22.4	49.5	41.2
COE2	15	7.5	20.8	38.3	47.5
COE3	15	5	19	43.9	37.6

**Table 8**  
A comparison between the results of RSM and outputs of LS-DYNA for absorbers with open-ended cap.

	SEA (J/g)	Fm (kN)
Crushing properties of proposed absorber by RSM method	22.52	40
Crushing properties of simulated absorber by LS-DYNA	20.6	42.3
Difference (%)	-8.5	5.8

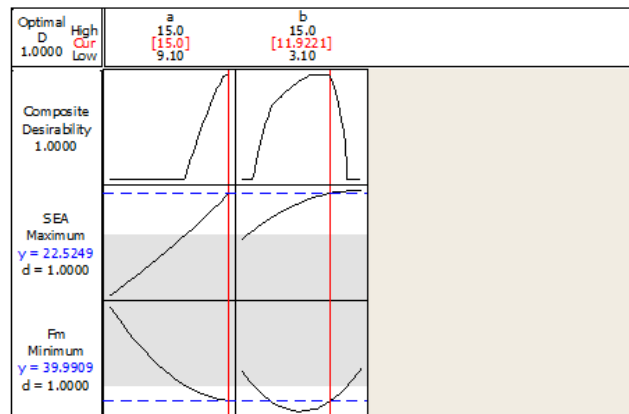


**Fig. 14.** Optimization results with RSM for absorbers with open-ended cap (Using SEA and Fm).

In Fig. 14, some curves are plotted for dependent variables (functions) of D, SEA and Fm versus independent variables of “a” and “b”. These plots show the schematic changes of functions versus “a” and “b”. Vertical red line in each curve of Figure 14 is for showing the optimal amounts of “a” and “b” in which the optimal state of SEA and Fm are proposed. The parameter of D is a desirability function of SEA and Fm and usually would be used in single-objective and multi-objective optimization in Minitab software. This function would be defined according to reference [20] and its variation is between 0 and 1. If desirability function is equal to 1, the best optimum would be achieved for SEA and Fm. According to Fig. 14 for the values 15 and 11.9221 for the parameters of “a” and “b”, the

desirability function would be equal to 1. Extended information about desirability function can be found in reference [20].

$$SEA = 25.07 - 1.5a - 1.48b + 0.05a^2 - 0.04b^2 + 0.17ab \quad (3)$$

$$R^2 = 0.905$$

$$Fm = 33.96 - 9.34a + 11.328b + 0.77a^2 + 0.38b^2 + 1.21ab \quad (4)$$

$$R^2 = 0.959$$

Instead of multi-objective optimization using SEA and Fm, a multi-objective problem with SEA and CFE can be investigated. Both SEA and CFE parameters must be maximized; for this purpose, crush force efficiency of the absorbers with open-ended caps is expressed as Eq. (5). The result of multi-objective optimization via RSM for SEA and CFE is shown in Fig. 15. As shown in this figure, the values of 15 and 10.43 of “a” and “b” leads to a specific energy absorption of 22.1 and a crush force efficiency of 52.9, respectively. These results indicate a circular form for the main tube section ( $a = 15$ ) and a circular cap with an upper base of 20.86mm in radius ( $b = 10.43$ ) which is very similar to the results of multi objective optimization with SEA and Fm.

$$CFE = 106.85 + 2.91a - 18.03b + 0.68a^2 - 0.51b^2 + 1.91ab \quad (5)$$

$$R^2 = 0.91$$

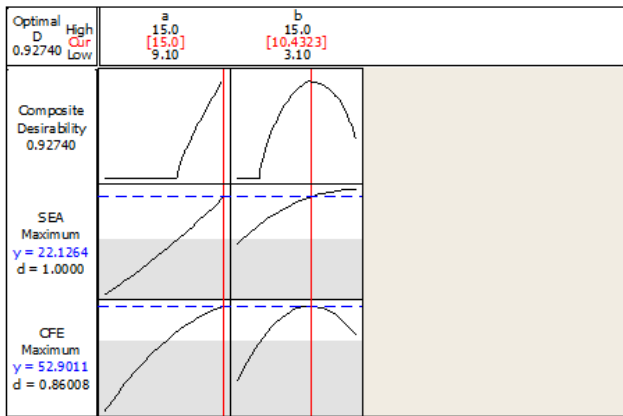


Fig. 15. Optimization results by RSM for absorbers with open-ended cap (Using SEA and CFE).

4.2.2. Optimization of Absorbers with Close-ended Caps

Table 9 lists the parameters used to optimize the absorbers with close-ended cap. Based on this table and using RSM, two quadratic equations were determined for specific energy absorption and maximum force at collapse of the absorbers with close-ended caps, namely Eqs. (6) and (7), respectively. Indicated beside each equation is the corresponding value of R2. It should be noted that, in cases where the value of R2 was found to be lower than 0.9, it is necessary to propose another

function for describing the collapse behavior of the energy absorber. Fig. 16 demonstrates the surfaces and contours corresponding to Eqs. (6) and (7).

Fig. 17 shows the results of multi-objective optimization via RSM. Given this figure, the absorber with “a” and “b” values of 17.94 and 7.85 was expected to exhibit specific energy absorption and maximum force at collapse of 19.80 and 41, respectively. The value of the parameter “a” (14.94) refers to an approximately circular form for the main tube section; as such, the main tube and hence the cap should be selected with circular sections. The value of the parameter “b” (7.85) defines a circular cap with a base of 15.7mm in radius. In order to verify the predictions obtained from the RSM, the proposed absorber was simulated in LS-DYNA. Table 10 compares the results of RSM with the outputs of LS-DYNA, indicating the capability of the RSM in predicting the optimal configuration for close-ended structures.

$$SEA = 15.64 - 0.52a - 0.28b - 0.04a^2 + 0.01b^2 + 0.04ab \quad (6)$$

$$R^2 = 0.928$$

$$Fm = 25.98 - 3.86a + 5.8b + 0.36a^2 + 0.18b^2 + 0.55ab \quad (7)$$

$$R^2 = 0.939$$

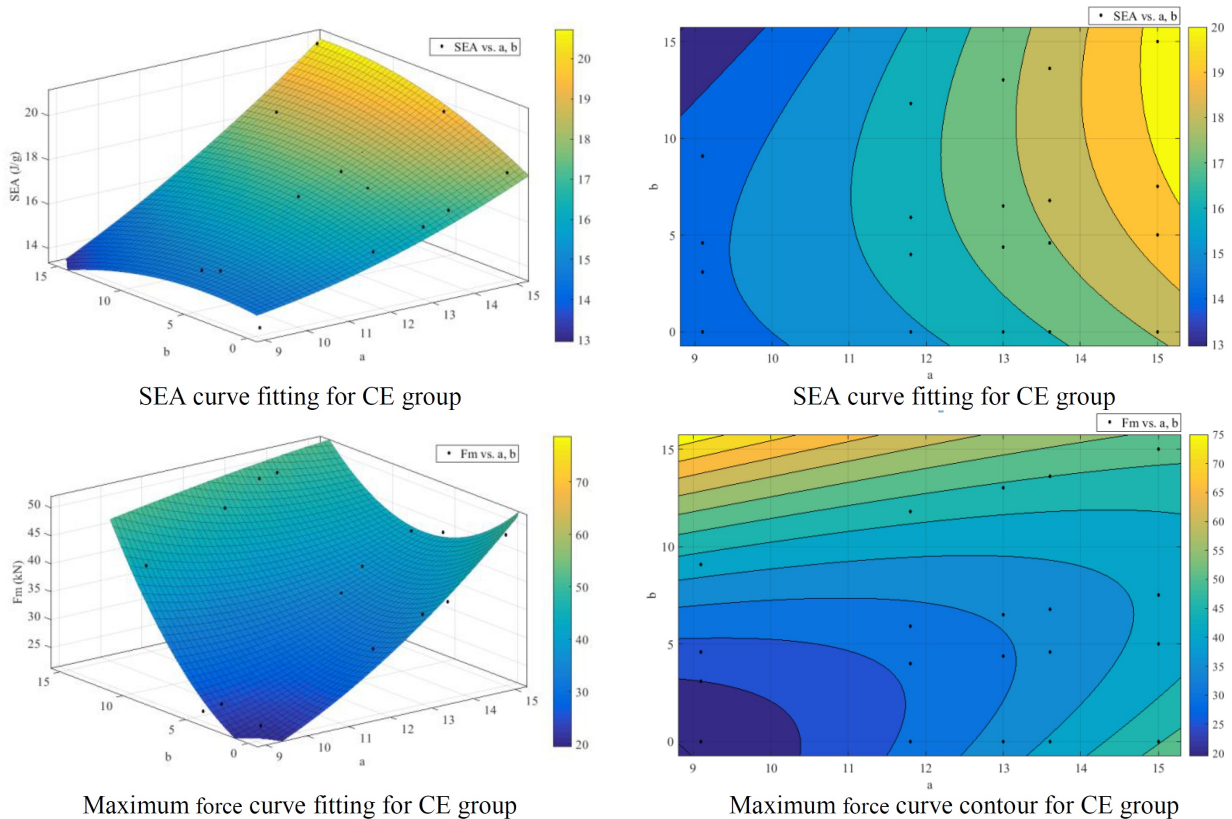


Fig. 16. The fitted curve and corresponding contours for specific energy absorption and maximum force at collapse of absorbers with close-ended cap.

**Table 9**  
The parameters used to optimize the absorbers with close-ended cap.

Specimen	a	b	SEA (J/g)	Fm (kN)	CFE (%)
TCE1	9.1	9.1	14.2	44.8	31
TCE2	9.1	4.6	15.3	22.7	59.5
TCE3	9.1	3.1	15.6	25.2	52.8
TCE4	9.1	0	13.7	24	46.7
QCE1	11.8	11.8	16.1	48.3	33.1
QCE2	11.8	5.9	17.2	30.1	50.8
QCE3	11.8	4	16.3	30.2	46.7
QCE4	11.8	0	16	33.2	39.8
PCE1	13	13	17.5	50.6	35.4
PCE2	13	6.5	17.7	35.6	44.7
PCE3	13	4.4	17.4	33.4	45.8
PCE4	13	0	16.6	37.4	37.4
HCE1	13.6	13.6	18.6	50.2	37.1
HCE2	13.6	6.8	18.2	39.2	41.3
HCE3	13.6	4.6	17.7	35.3	43.1
HCE4	13.6	0	17.1	38.6	36.5
CCE1	15	15	20.8	49.4	43.1
CCE2	15	7.5	18.8	42.6	39.9
CCE3	15	5	19.9	44.5	39.3
CCE4	15	0	18.2	48.3	31.9

**Table 10**  
A comparison between the results of RSM and outputs of LS-DYNA for absorbers with close-ended cap.

	SEA (J/g)	Fm (kN)
Crushing properties of proposed absorber by RSM method	19.8	41
Crushing properties of simulated absorber by LS-DYNA	18.9	42.9
Difference (%)	-4.5	4.6

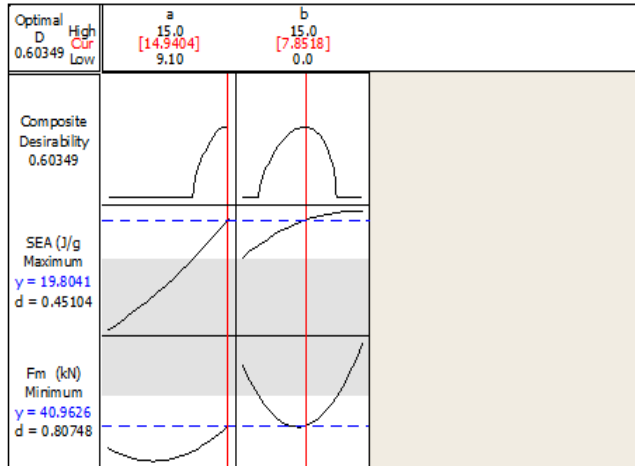


**Fig. 17.** Optimization results with outputs of RSM for absorbers with close-ended cap (Using SEA and Fm).

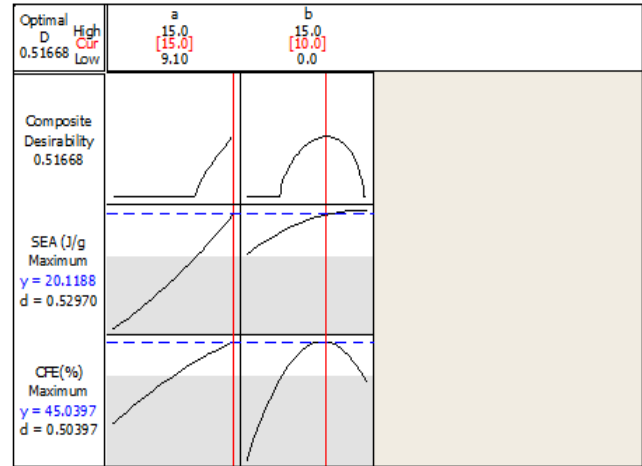


**Fig. 18.** Optimization results with outputs of RSM for absorbers with close-ended cap (Using SEA and CFE).

Crush force efficiency of the absorbers with close-ended caps is expressed as Eqs. (8). The result of multi-objective optimization via RSM for SEA and CFE is shown in Fig. 18. The proposed absorber is a structure with a circular form for the main tube section ( $a = 15$ ) and a circular cap with an upper base of 20mm in radius ( $b = 10$ ), the SEA and CFE of

the proposed absorber is 20.11(J/g) and 45%, respectively. Results show that the proposed absorber using SEA and CFE is far better in energy absorption.

$$CFE = 76.76 - 1.59a - 5.7a - 0.11a^2 - 0.18b^2 + 0.61ab \tag{8}$$

$$R^2 = 0.93$$

## 5. Conclusions

In the present study, a special type of energy absorber was investigated. This type of absorber is made up of two parts: (1) a main tube, and (2) a cap. The cap has been used to reduce the maximum force at collapse. Five section geometries and seven cap geometries were considered to develop a total of 35 different cases to test. The present study was performed both numerically and experimentally. The numerical analyses were performed by LS-DYNA software. Upon comparing the numerical results to the corresponding experimental data, the software was found to be well capable of simulating capped absorbers under quasi-static loading. In the final stage of the study, optimal absorbers for the cases with open-ended and close-ended caps were proposed using Minitab Software and response surface methodology. The results were in good agreement with those of LS-DYNA. The results of the present research showed that, in all cases, the application of a cap brings about enhanced crush force efficiency (CFE) while reducing maximum force at collapse.

## References

- [1] W. Abramowicz, The effective crushing distance in axially compressed thin-walled metal columns, *Int. J. Impact Eng.*, 1(3) (1983) 309-317.
- [2] W. Abramowicz, N. Jones, Dynamic axial crushing of circular tubes, *Int. J. Impact Eng.*, 2(3) (1984) 263-281.
- [3] T. Wierzbicki, W. Abramowicz, On the crushing mechanics of thin-walled structures, *J. Appl. Mech.*, 50(4a) (1983) 727-734.
- [4] M. Güden, H. Kavi, Quasi-static axial compression behavior of constraint hexagonal and square-packed empty and aluminum foam-filled aluminum multi-tubes, *Thin Walled Struct.*, 44(7) (2006) 739-750.
- [5] A.G. Olabi, E. Morris, M.S.J. Hashmi, M.D. Gilchrist, Optimised design of nested circular tube energy absorbers under lateral impact loading, *Int. J. Mech. Sci.*, 50(1) (2008) 104-116.
- [6] M. Avalle, G. Chiandussi, Optimisation of a vehicle energy absorbing steel component with experimental validation, *Int. J. Impact Eng.*, 34(4) (2007) 843-858.
- [7] X.W. Zhang, Q.D. Tian, T.X. Yu, Axial crushing of circular tubes with buckling initiators, *Thin Walled Struct.*, 47(6-7) (2009) 788-797.
- [8] E. Acar, M.A. Guler, B. Gerçeker, M.E. Cerit, B. Bayram, Multi-objective crashworthiness optimization of tapered thin-walled tubes with axisymmetric indentations, *Thin Walled Struct.*, 49(1) (2011) 94-105.
- [9] M. Shariati, H.R. Allahbakhsh, Numerical and experimental investigations on the buckling of steel semi-spherical shells under various loadings, *Thin Walled Struct.*, 48(8) (2010) 620-628.
- [10] A. Alavi Nia, J. Haddad Hamedani, Comparative analysis of energy absorption and deformations of thin walled tubes with various section geometries, *Thin Walled Struct.*, 48(12) (2010) 946-954.
- [11] A. Ghamarian, M.A. Farsi, Experimental and numerical analysis of collapse behavior of combined Thin walled structures under axial loading, *Aerosp. Res. Inst.*, 8 (2012) 99-109.
- [12] A. Ghamarian, M. Tahaye Abadi, Axial crushing analysis of end-capped circular tube, *Thin Walled Struct.*, 49(6) (2011) 743-752.
- [13] V. Jandaghi Shahi, J. Marzbanrad, Analytical and experimental studies on quasi-static axial crush behavior of thin-walled tailor-made aluminum tubes, *Thin Walled Struct.*, 60 (2012) 24-37.
- [14] J. Song, Numerical simulation on windowed tubes subjected to oblique impact loading and a new method for the design of obliquely loaded tubes, *Int. J. Impact Eng.*, 54 (2013) 192-205.
- [15] G. Sun, F. Xu, G. Li, Q. Li, Crashing analysis and multiobjective optimization for thin-walled structures with functionally graded thickness, *Int. J. Impact Eng.*, 64 (2014) 62-74.
- [16] S. Sharifi, M. Shakeri, H.E. Fakhari, M. Bodaghi, Experimental investigation of bitubal circular energy absorbers under quasi-static axial load, *Thin Walled Struct.*, 89 (2015) 42-53.
- [17] A. Alavi Nia, S. Chahardoli, Optimizing the layout of nested three-tube structures in quasi-static axial collapse, *Thin Walled Struct.*, 107 (2016) 169-181.
- [18] A.S.M.I.H. Committee, Properties and Selection: Nonferrous Alloys and Special- Purpose Materials: ASM International, (1990).
- [19] ASTM. International, ASTM E8/E8M - 09 Standard Test Methods for Tension Testing of Metallic Materials: ASTM, (2009).
- [20] R. Suich, G. Derringer, Simultaneous optimization of several response variables, *J. Qual. Tech.*, 12(4) (1980) 214-219.